ACS APPLIED MATERIALS & INTERFACES

Research Article

www.acsami.org

Construction of Planar and Bulk Integrated Heterojunction Polymer Solar Cells Using Cross-Linkable D-A Copolymer

Qi Xu,[†] Fuzhi Wang,[†] Deping Qian,[†] Zhan'ao Tan,*[,†] Liangjie Li,[†] Shusheng Li,[†] Xiaohe Tu,[†] Gang Sun,[†] Xuliang Hou,[†] Jianhui Hou,*[,‡] and Yongfang Li*[,‡]

[†]State Key Laboratory of Alternate Electrical Power System with Renewable Energy Sources, the New and Renewable Energy of Beijing Key Laboratory, North China Electric Power University, Beijing 102206, People's Republic of China

[‡]Beijing National Laboratory for Molecular Sciences, Institute of Chemistry, Chinese Academy of Sciences, Beijing 100190, People's Republic of China

ABSTRACT: An integrated device architecture was constructed via vertical combination of planar and bulk heterojunctions by solution processing, where a cross-linked D-A copolymer (PBDTTT-Br25) was inserted between a PEDOT:PSS layer and the blended photoactive layer. PBDTTT-Br25 can readily undergo photo crosslinking to form an insoluble robust film via ultraviolet irradiation after solution−deposition, which enables the subsequent solution processing of a photoactive layer on the robust surface. The insertion of a pure PBDTTT-Br25 layer to build an integrated heterojunction could provide an additional donor/acceptor interface, which enables hole transport to the anode without interruption, thereby reducing the charge carrier recombination probability. The power conversion efficiency (PCE) of the polymer solar cell (PSC) with the integrated architecture reaches 5.24% under an AM1.5G illumination of 100 mW/cm^2, which is increased by 65%, in comparison with that of the reference single heterojunction device (3.17%), under the same experimental conditions.

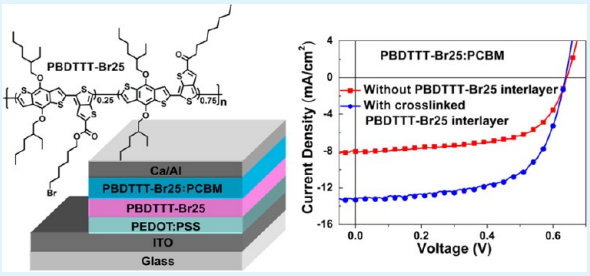

KEYWORDS: *planar solar cells, bulk heterojunction solar cells, integrated architecture, D-A copolymer, photo-cross-linkable conjugated polymers*

1. INTRODUCTION

Polymer solar cells (PSCs) have gained extensive attention in recent years, because of their potential applications.[1,2] In order to increase the donor/acceptor contact area for efficient charge separation, a bulk-heterojunction (BHJ) structure has been introduced to form a nanoscale interpenetrating network of donor and acceptor materials.[3−6] The advantage of the BHJ configuration is the increase of the donor/acceptor interface area, so that most of the excitons could reach the heterojunction interface within exciton diffusion length, which is beneficial to improving the exciton separation efficiency. However, a critical issue for bulk heterojunction PSCs is that the physical blending of donor and acceptor materials could result in macrophase separation. The domain sizes of donor or acceptor phase could exceed the exciton diffusion length (ca. 10 nm), and there could exist randomly distributed floating islands or dead ends (donor or acceptor domains that are isolated and not connected to the electrodes) in the active layer, which hinder the separated charge from transporting to the respective electrodes.[7−9] Therefore, the electrons generated near the anode and the holes generated near the cathode could not transport to the corresponding electrodes to be efficiently collected, which leads to increased charge recombination and reduced current.[1,10,11] One approach to overcome this drawback is to construct ordered BHJ films,[12] which would enhance the charge transport and collection. Unfortunately, it is difficult to demonstrate such a structure in the BHJ system. On the contrary, in conventional planar solar cells, electrons and holes have their own respective transport channel; therefore, the carrier collection efficiency on the electrodes of the planar devices is much higher than that of BHJ devices. A further improvement strategy is the construction of planar and bulk integrated heterojunction polymer solar cells.[13−18] The idea is to produce a series of stacked layers bearing different functions. The implementation of planar and bulk integrated heterojunction offers many advantages over the single planar and bulk heterojunctions, i.e., (1) a spatially continuous pathway for the transport of charge carriers to their corresponding electrodes, thus charge recombination at the electrodes can be reduced; (2) an extra donor/acceptor interface which could increase the probability of exciton dissociation; (3) the absorbing layer thickness can be optimized to achieve better quantum efficiency; (4) it is possible to tune the internal distribution of the electrical field within the different layers.[13,18] However, it is a challenge to fabricate well-organized multilayer devices with commonly used materials (e.g., P3HT and PCBM) via solution processing, since most organic solvents used for the formation of the upper layer can dissolve the previously coated

Received: April 7, 2013
Accepted: June 19, 2013
Published: June 19, 2013

underneath layer, which destroys the orthogonal structure.[17,19] An approach to solve the dissolution problem in solution processed multilayer devices is utilization of cross-linkable materials, which can readily undergo chemical crosslinking to form insoluble films through thermal treatment or UV irradiation. Such materials would therefore enable the sequential deposition of several layers and also improve the thermal stability of the device.[15,20−22] The photo-crosslinkable materials can be crosslinked through photoinitiation with minimal effect on the packing of conjugated polymers and electronic properties, thus enabling high performing and thermally stable PSCs. However, the currently reported crosslinkable materials merely acted as buffer layers, wherein the transportation of the selective carriers could be increased, thus the device performance could be improved by reducing separated charge quenching. Poly[4,8-bis-substituted-benzo-[1,2-b:4,5-b′]dithiophene-2,6-diyl-alt-4-substituted-thieno[3,4-b]thiophene-2,6-diyl] (PBDTTT)-derived polymers are a type of narrow-band-gap D-A copolymer with excellent optical and electronic properties.[23] The photo-cross-linkable conjugated polymer, PBDTTT-Br25, with conjugated backbone and bromine-functionalized side group, can be cross-linked through photoinitiation with minimal effect on the packing of conjugated polymers and electronic properties.

Herein, we insert the cross-linkable PBDTTT-Br25 layer between the indium tin oxide (ITO) anode and the blend active layer to produce a vertical integrated structure of planar and bulk heterojunction. In addition to serving as the buffer layer, the additional PBDTTT-Br25 layer can also serve as a donor layer to form an extra planar heterojunction with the PCBM acceptor molecules at the bottom of the blend active layer. The integrated planar and bulk heterojunction could create an extra donor/acceptor interface for more-efficient exciton dissociation and carrier collection. The PSC with integrated architecture exhibits higher short-circuit current density (J_{sc}) and input photon to converted current efficiency (IPCE), compared to a single heterojunction device. The extra planar structure increases the extraction of holes by decreasing the charge recombination at the anode. The power conversion efficiency (PCE) of the PSC was improved by 65%, from 3.17% to 5.24%, using this integrated structure of planar and bulk heterojunctions.

2. EXPERIMENTAL DETAILS

ITO-coated glass substrates (series resistance, R_s = 10 Ω/□, CSG Holding Co., Ltd.) was used as the anode. PEDOT:PSS (Clevious P VP AI 4083, H. C. Starck, Inc.) was chosen as the hole-transport layer. PCBM was purchased from Nano-C. 1,8-Diiodooctane (DIO) was purchased from Alfa Aesar. PBDTTT-Br25 was synthesized by Stille cross-coupling polymerization in our group, according to previously reported procedures.[24] The weight-average molecular weight (M_w) and polydispersity index (PDI) of PBDTTT-Br25 are 3.1×10^4 and 2.0, respectively.

An Ambios Technology XP-2 surface profilometer was used to measure the thickness of the films. Topographic and phase images of films were analyzed using a VEECO DICP-II atomic force microscopy (AFM) system operated in the tapping mode. The absorption spectrum of PBDTTT-Br25 film was recorded on a Hitachi U-3010 UV-Vis spectrophotometer. The cross-section morphologies were observed using a Hitachi S-4800 cold-field-emission scanning electron microscopy (SEM) system.

Device fabrication process has been described in a previous paper.[29] The PSCs were fabricated with three types of structures: A, a control single bulk heterojunction device, ITO/PEDOT:PSS (30 nm)/PBDTTT-Br25:PCBM (90 nm)/Ca (10 nm)/Al (100 nm); B and C, integrated architecture device, ITO/PEDOT:PSS (30 nm)/PBDTTT-Br25 (5−18 nm)/PBDTTT-Br25:PCBM (90 nm)/Ca (10 nm)/Al (100 nm). The difference between devices B and C is that the pure PBDTTT-Br25 layer in device B is not photo-cross-linked, whereas for device C, the pure PBDTTT-Br25 layer is cross-linked by UV radiation. The PSCs were fabricated on a patterned ITO substrate, which had been cleaned by sequential ultrasonic treatment in detergent, deionized water, acetone, and isopropanol. Then, the ITO substrate was subjected to UV−ozone treatment for 20 min. After that, a PEDOT:PSS film was prepared by spin coating an aqueous solution of PEDOT:PSS at 2000 rpm for 60 s on the pre-cleaned ITO electrode, and then baked at 150 °C for 10 min in air. The pure PBDTTT-Br25 layer was prepared by spin-coating a 12 wt % PBDTTT-Br25 1,2-dichlorobenzene solution onto a ITO/PEDOT substrate and then baking it at a low temperature of 150 °C for 10 min. The thickness of the pure PBDTTT-Br25 layer was controlled from 5 nm to 18 nm by modifying the concentration of the PBDTTT-Br25 solution and the spin-coating rate. For device C, photo-crosslinking was carried out for the PBDTTT-Br25 layer in a nitrogen-filled glove box, using 254-nm UV light from a low-power handheld lamp for 10 min to produce an insoluble film, enabling the fabrication of the subsequent blended layer by spin-coating. The same procedure was conducted for the preparation of the active layer for the three types of PSCs: a solution containing a mixture of PBDTTT-Br25:PCBM (1:1.5 w/w, polymer concentration of 10 mg/mL) in 1,2-dichlorobenzene with 2.5 vol % DIO was then spin-coated (2000 rpm) for 60 s on top of the PEDOT:PSS or PEDOT:PSS/PBDTTT-Br25 layer. DIO was used as an additive to optimize the active layer morphology. Then, 10 nm of calcium and 100 nm of aluminum were deposited sequentially, through vapor deposition.

Device characterization was done in a nitrogen-filled glove box under a simulated AM1.5G irradiation of 100 mW/cm^2, using a xenon-lamp-based solar simulator (Newport Co., Ltd.). The current density−voltage (J−V) measurement of the devices was conducted on a computer-controlled Keithley 236 Source Measure Unit. IPCE measurement was performed with a Stanford Research System model SR830 DSP lock-in amplifier coupled with a WDG3 monochromator and a 500-W xenon lamp under ambient atmosphere at room temperature. The light intensity at each wavelength was calibrated with a standard single-crystal Si photovoltaic cell.

3. RESULTS AND DISCUSSION

The molecular structure of PBDTTT-Br25 is given in Figure 1a. PSCs were fabricated with the configuration of ITO/PEDOT:PSS/PBDTTT-Br25/PBDTTT-Br25:PCBM/Ca/Al, where PEDOT:PSS was selected as the hole collection layer and PBDTTT-Br25:PCBM was used as the photoactive layer. An underlying pure PBDTTT-Br25 layer inserted between the PEDOT:PSS hole collection layer and the photoactive layer forms an additional planar heterojunction with PCBM molecules present at the bottom of the blend layer. The pure PBDTTT-Br25 layer can facilitate charge separation and transport at the PBDTTT-Br25/PBDTTT-Br25:PCBM interface, while avoiding the carrier recombination at the anode. For comparison, a reference device with a single bulk heterojunction was also fabricated, in parallel with the structure of ITO/PEDOT:PSS/PBDTTT-Br25:PCBM/Ca/Al. Figure 1b depicts the simplified energy band diagram of the device. The electronic energy levels of PBDTTT-Br25 and PCBM were taken from the literature.[24,25]

When light irradiates the active layers through the ITO electrode, the pure PBDTTT-Br25 layer and the PBDTTT-Br25:PCBM blend layer will absorb photons to produce excitons at the same time. Excitons generated in the blend layer can diffuse efficiently to the bulk heterojunction interfaces to be separated into holes and electrons. At the same time, the excitons generated in the pure PBDTTT-Br25 layer can diffuse

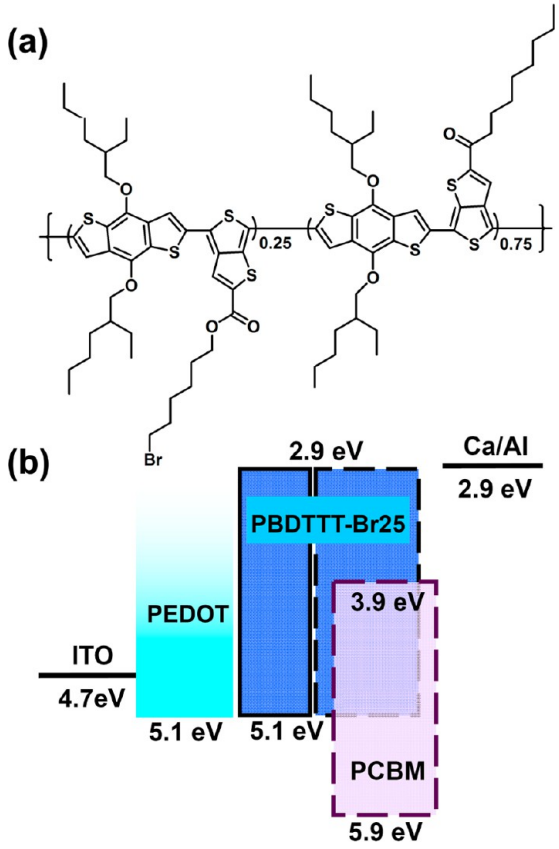

Figure 1. (a) Molecular structure of PBDTTT-Br25. (b) Highest occupied molecular orbital (HOMO) and lowest unoccupied molecular orbital (LUMO) energy levels of the materials involved in the polymer solar cells (PSCs).

to the planar heterojunction interface, to be separated into holes and electrons. The pure PBDTTT-Br25 interlayer also provides a straight and independent pathway for holes to the anode. With the integrated structure of planar and bulk heterojunctions, electrons and holes can effectively transport to the corresponding electrode with the minimized recombination losses.

Since the HOMO of the PBDTTT-Br25 (−5.06 eV) is very close to that of the PEDOT:PSS, an ohmic contact can be formed between the pure PBDTTT-Br25 interlayer and the PEDOT:PSS layer. The LUMO level of PBDTTT-Br25 (−2.92 eV) is much higher than that of PCBM (−3.9 eV), so that it blocks the electron transport from PCBM to the anode. Therefore, the device efficiency can be increased through insertion of this pure PBDTTT-Br25 layer by decreasing the recombination of the separated charges.

The layer of PBDTTT-Br25:PCBM blend on the underlying un-cross-linked (sample B) or cross-linked (sample A) PBDTTT-Br25 have been examined by cross-sectional SEM (Figure 2). For the sake of convenience of the test, the thicknesses of the pure PBDTTT-Br25 and the blend layer here are different from those of the corresponding layers used in the device. The pure PBDTTT-Br25 layer was prepared by spin-coating a 24 mg/mL PBDTTT-Br25 1,2-dichlorobenzene solution on the pre-cleaned glass substrate, and then baked at 150 °C for 10 min. For sample A, as shown in Figure 2a, in situ crosslinking of the underlying PBDTTT-Br25 was carried out by UV exposed after heating at 150 °C for 10 min to achieve an insoluble film. In contrast, the underlying PBDTTT-Br25 film was not cross-linked for sample B, as shown in Figure 2b. A PBDTTT-Br25:PCBM blend layer was prepared by spin-coating a solution containing a mixture of PBDTTT-Br25:PCBM in 1,2-dichlorobenzene on top of the cross-linked or as-prepared (un-cross-linked) PBDTTT-Br25 layer. SEM analysis shows that a sharp interface was formed between the two layers of PBDTTT-Br25 and PBDTTT-Br25:PCBM for sample A (as shown in Figure 2a), which suggested that, after crosslinking, the underlying PBDTTT-Br25 layer could remain undissolved under the solution deposition of the upper blend layer. In contrast, the un-cross-linked PBDTTT-Br25 film was intermixed with the upper layer during the solution deposition process of the upper layer, leading to a blurred-edge region, as shown in Figure 2b. The results show that crosslinking the PBDTTT-Br25 layer can solve the dissolution problem when preparing multilayer devices with the solution process, thereby enabling the sequential deposition of several layers and also potentially improving the thermal stability of the device.

Figure 3a and 3b show the tapping-mode AFM images of PEDOT:PSS on ITO and PBDTTT-Br25 interface layer on ITO/PEDOT:PSS crosslinked by UV exposed after heating at 150 °C for 10 min, respectively. The root-mean-square (rms) roughness of the pure PBDTTT-Br25 layer is only 0.92 nm, which is small compared with that of the ITO/PEDOT:PSS substrate (1.73 nm). The results demonstrate that a smoother

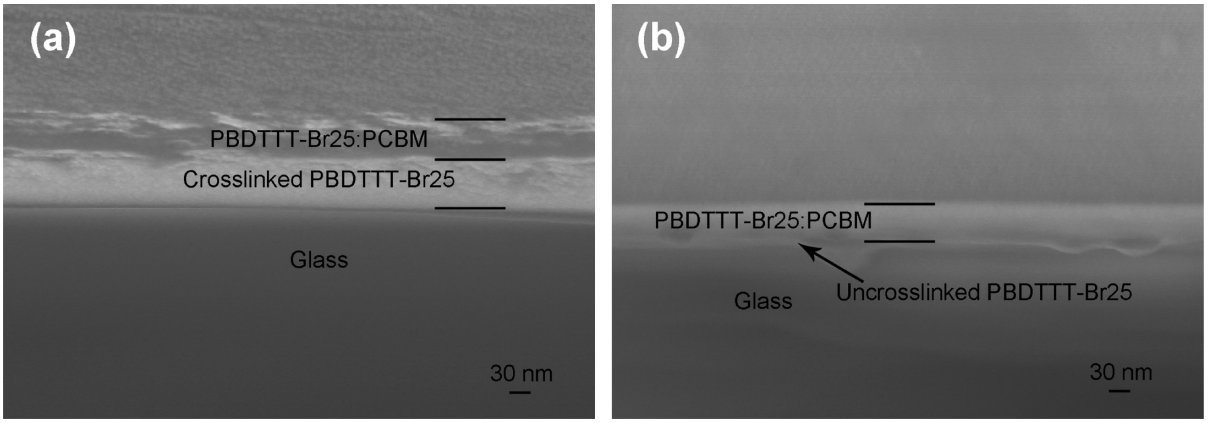

Figure 2. Cross-sectional scanning electron microscopy (SEM) micrograph of (a) cross-linked PBDTTT-Br25/PBDTTT-Br25:PCBM and (b) un-cross-linked PBDTTT-Br25/PBDTTT-Br25:PCBM.

dx.doi.org/10.1021/am401263m | ACS Appl. Mater. Interfaces 2013, 5, 6591−6597

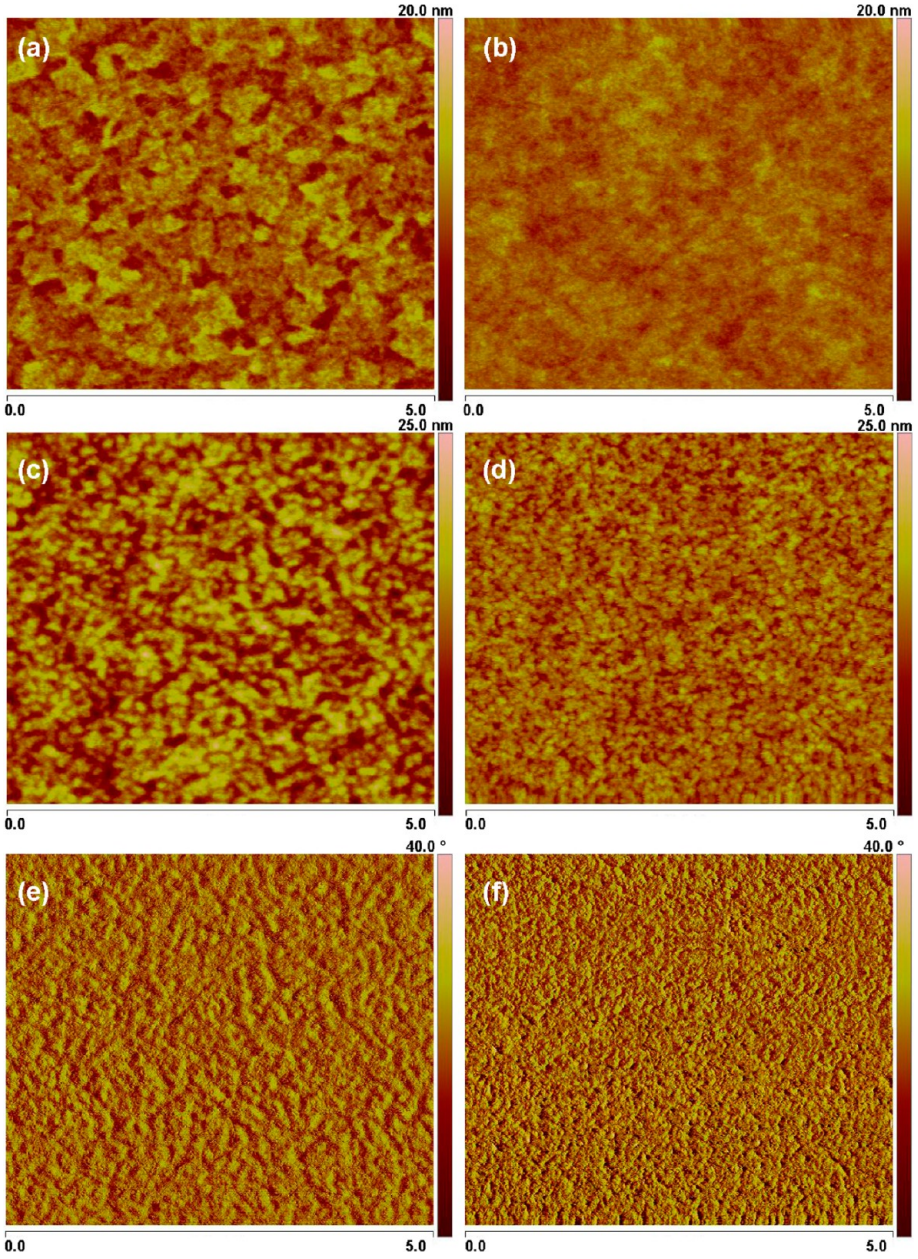

Figure 3. AFM images of (a) ITO/PEDOT:PSS, (b) ITO/PEDOT:PSS/PBDTTT-Br25, (c) and (e) PBDTTT-Br25:PCBM (1:1.5, w/w) on ITO/PEDOT:PSS substrate, (d) and (f) PBDTTT-Br25:PCBM (1:1.5, w/w) on ITO/PEDOT:PSS/PBDTTT-Br25 substrate, with a scan size of 5 μm × 5 μm. Panels (a), (b), (c), and (d) are height images; panels (e) and (f) are phase images.

surface can be achieved by applying the PBDTTT-Br25 interlayer, which enables a more uniform interfacial contact between the buffer layer and blend active layers, thus increasing the hole collection efficiency and affecting the morphology of the upper active layer, as shown in Figures 3c–f. The height image of the surface of the blend layer on PEDOT:PSS substrate shows an rms roughness of 2.99 nm (see Figure 3c). The use of the intermediate PBDTTT-Br25 layer can improve the flatness of the blend layer (rms roughness of 1.89 nm). In traditional P3HT:PCBM-based BHJ cells, the spin-coated film is not exactly a uniform blend of donor and acceptor, in which the thermodynamically favored vertical stratification consists of a uniformly blended "bulk" structure capped with a P3HT-rich air interface and a slightly PCBM-rich region at the bottom of the blend layer.[32,33] The vertical material gradient could be ascribed to differences in the surface energies of the ingredients: P3HT (23.2 mN/m^2) shows a lower surface energy than that of PCBM (45.1 mN/m^2).[33] The surface energy of PBDTTT-Br25 was determined to be 18.04 mN/m^2 using the Owens–Wendt method,[34] which is lower than that of P3HT. Therefore, we infer that there is similar vertical stratification in the PBDTTT-Br25:PCBM blend layer, according to the comprehensive free-energy analysis. The smooth surface of PBDTTT-Br25 enables the formation of a well-organized planar heterojunction between the pure PBDTTT-Br25 layer and the fullerene acceptor molecules that exist at the bottom of the blend film.

Phase separation can occur during the film-forming process, which means that the aggregation of PBDTTT-Br25 and PCBM molecules can form separated continuous paths for the transport of holes and electrons. As shown in Figures 3c and 3d, AFM images clearly reveal the strong influence of insertion of the pure PBDTTT-Br25 interlayer. Figures 3e and 3f are

phase images of PBDTTT-Br25:PCBM film on the ITO/PEDOT:PSS substrate and on the ITO/PEDOT:PSS/PBDTTT-Br25 substrate, separately. Generally, the phase image can give a picture of the change in surface local hardness.[26] For the polymer−fullerene mixture system, the phase contrast image can be interpreted as showing fullerene-rich and fullerene-poor domains.[27]

The $J-V$ curves of the PSCs in darkness and under an AM1.5G illumination of 100 mW/cm^2 are shown in Figure 4a.

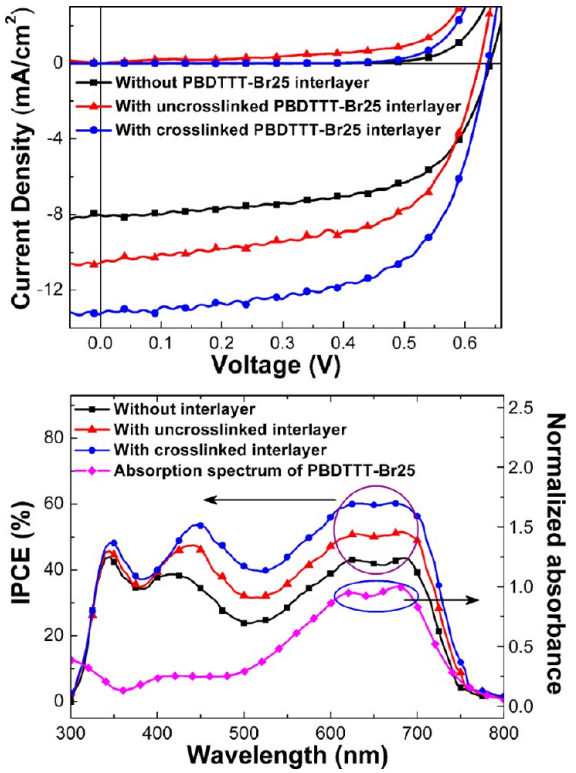

Figure 4. (a) Current density−voltage curves of the PSCs (devices A−C) under an AM 1.5G illumination of 100 mW/cm^2; (b) IPCE spectra of the PSCs and absorbance of the PBDTTT-Br25 film.

Table 1. Device Parameters of Devices A−C in Darkness and under an Illumination of 100 mW/cm^2

device	open-circuit voltage, V_{oc} (V)	short-circuit current density, J_{sc} (mA/cm^2)	fill factor, FF (%)	power conversion efficiency, PCE (%)	series resistance, R_s[a] (Ω cm^2)
A	0.64	8.04	61.6	3.17	3.1
B	0.62	10.58	60.1	3.94	2.0
C	0.64	13.32	61.5	5.24	1.3

[a]The series resistance for PSCs in darkness is obtained at ∼1 V.

The device parameters are summarized in Table 1. Device A, without the PBDTTT-Br25 interlayer, shows a PCE of 3.17%, a J_{sc} of 8.04 mA/cm^2, an open-circuit voltage (V_{oc}) of 0.64 V, and a fill factor (FF) of 61.6%. For device B, the un-cross-linked PBDTTT-Br25 film was intermixed with the solution-deposited upper layer (as shown in Figure 2b); therefore, device B shows only slightly higher performance with a PCE of 3.94%, a J_{sc} value of 10.58 mA/cm^2, while the V_{oc} value is slightly decreased to 0.62 V. From the relatively small improvement in the performance of device B, we can conclude that, although the morphology of un-cross-linked PBDTTT-Br25 was partly destroyed by the deposition of the upper layer, the remnant of the PBDTTT-Br25 layer can still play an important role in improving the hole collection efficiency. In contrast, the spin-coating process of the top blended layer could not damage the morphology of the cross-linked PBDTTT-Br25 layer for device C. Thus, an additional well-organized planar heterojunction formed between the pure PBDTTT-Br25 layer and the fullerene acceptor molecules that exist at the bottom of the blend film. Device C exhibits greatly improved performance compared with the device without the PBDTTT-Br25 interlayer. Device C shows a PCE of 5.24%, with J_{sc} = 13.32 mA/cm^2, V_{oc} = 0.64 V, and FF = 61.5%, both J_{sc} and PCE are increased for device C, while the FF and V_{oc} values are almost the same. As shown in Figure 4a and Table 1, the enhanced PCE in device C mainly originates from the increase of J_{sc}. The total R_s for PSCs in darkness is calculated from the $J-V$ characteristic at ∼1 V. The R_s value of device A without the PBDTTT-Br25 interlayer is ∼3.1 Ω cm^2, while that of device C, with the cross-linked PBDTTT-Br25 interlayer, is decreased to 1.3 Ω cm^2. The results prove that the planar heterojunction could reduce the interface resistance between the active layer and ITO/PEDOT:PSS anode, leading to a higher J_{sc}. This enhancement could be ascribed to that the pure PBDTTT-Br25 interfacial layer could provide a straight pathway for holes transport and the consequent reduction of contact resistance and minimization of recombination losses.

To further understand the enhanced J_{sc} value in device C, we compared the IPCE spectra of the three devices, as shown in Figure 4b. It can be seen that the maximum efficiency is reached for device C with integrated architecture. All the spectra show similar shapes; however, device C, with a crosslinked PBDTTT-Br25 interlayer, exhibits a much higher IPCE than the reference cell, which is consistent with the photocurrent enhancement shown in Figure 4a. All curves have peaks in the IPCE at ∼625 nm and ∼675 nm, which corresponds to the absorption maximum of the polymer. Remarkably, the characteristic signatures of PBDTTT-Br25 in the IPCE spectra between 550 nm and 750 nm become more pronounced from device A to device C. This change could be attributed to the extra excitons photogenerated in the underlying pure PBDTTT-Br25 layer and the additional planar heterojunction formed by the two adjacent layers.

The effects of the pure PBDTTT-Br25 interlayer thickness on the device performance were studied by changing the interlayer thickness. The $J-V$ characteristics for the polymer solar cells with different pure PBDTTT-Br25 thickness are shown in Figure 5, and the photovoltaic properties are listed in Table 2. The J_{sc} value of the device is gradually increased, while the V_{oc} value is almost the same. The V_{oc} is mainly decided by the energy difference between the HOMO of the donor material and the LUMO of the acceptor material; therefore, the V_{oc} is not affected by the thickness of the pure PBDTTT-Br25 interlayer. The insertion of pure PBDTTT-Br25 layer could provide an additional donor/acceptor interface, which enables the hole transport to the anode without interruption, thereby improving the exciton separation efficiency and reducing the charge carrier recombination probability. However, since the exciton life is very short, the diffusion length of an exciton in most conjugated polymer films is quite short (5−10 nm);[28−31] therefore, excessive thickness of the buffer layer will result in the excitons generated in the pure PBDTTT-Br25 interlayer

dx.doi.org/10.1021/am401263m | ACS Appl. Mater. Interfaces 2013, 5, 6591−6597

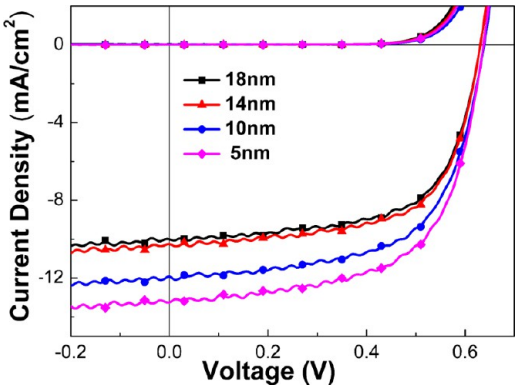

Figure 5. *J*–*V* curves of the PSCs with different PBDTTT-Br25 interlayer thickness in darkness and under an AM1.5G illumination of 100 mW/cm^2.

Table 2. Photovoltaic Performance of the PSCs with Different PBDTTT-Br25 Interlayer Thicknesses

thickness of PBDTTT-Br25 (nm)	open-circuit voltage, V_{oc} (V)	short-circuit current density, J_{sc} (mA/cm^2)	fill factor, FF (%)	power conversion efficiency, PCE (%)	series resistance, R_s[a] (Ω cm^2)
18	0.63	9.99	65.2	4.10	2.3
14	0.63	10.19	65.5	4.21	2.0
10	0.64	11.84	63.4	4.80	1.8
5	0.64	13.32	61.5	5.24	1.3

[a]The series resistance for PSCs in darkness is obtained at ~1 V.

failing to reach the donor/acceptor interface to be effectively dissociated. At the same time, excessive thickness of the buffer layer also increases the R_s of the device, as shown in Table 2. All of the above factors will decrease the J_{sc} value of the device, thus reducing the device efficiency. The optimal thickness of the PBDTTT-Br25 interlayer is <10 nm.

4. CONCLUSIONS

We demonstrated efficient planar and bulk integrated heterojunction PSCs with photo-cross-linked pure PBDTTT-Br25 as an additional hole collection layer. PBDTTT-Br25 could be readily cross-linked to form insoluble robust films via ultraviolet treatment after solution–deposition, which enables the preparation of multilayer devices via the solution method. The pure PBDTTT-Br25 interlayer shows good hole collection ability when the thickness of the PBDTTT-Br25 interlayer is <10 nm. The PCE of the PSC with a 5-nm pure PBDTTT-Br25 interlayer reached 5.24%, which is increased by 65%, compared to that of the device without a PBDTTT-Br25 interlayer (3.17%). The results indicate that the development of cross-linkable materials could provide an approach to construct multilayer cells with vertical integration of the planar and bulk heterojunctions by solution processing.

AUTHOR INFORMATION

Corresponding Author

*E-mail addresses: tanzhanao@ncepu.edu.cn (Z.A.T.), liyf@iccas.ac.cn (Y.F.L.), hjhzlz@iccas.ac.cn (J.H.H.).

Notes

The authors declare no competing financial interest.

ACKNOWLEDGMENTS

The work was supported by the NSFC (Nos. 21004019, 51173040, 91023039, and 21021091), the Ministry of Science and Technology of China (863 project, No. 2011AA050523) and the Chinese Academy of Sciences. Z.A.T. thanks the financial support from the Beijing NOVA Program (No. 2010B038), Program for New Century Excellent Talents in University (NCET-12-0848), SRFDP (No. 20100036120007), and Fundamental Research Funds for the Central Universities, China (Nos. 11QG18 and 13ZD11).

REFERENCES

(1) Günes, S.; Neugebauer, H.; Sariciftci, N. S. *Chem. Rev.* **2007**, *107*, 1324–1338.
(2) Li, Y. F. *Acc. Chem. Res.* **2012**, *45*, 723–733.
(3) Sariciftci, N. S.; Smilowitz, L.; Heeger, A. J.; Wudi, F. *Science* **1992**, *258*, 1474–1476.
(4) Yu, G.; Gao, J.; Hummelen, J. C.; Wudl, F.; Heeger, A. J. *Science* **1995**, *15*, 1789–1791.
(5) Chen, J. W.; Cao, Y. *Acc. Chem. Res.* **2009**, *42*, 1709–1718.
(6) Li, Y. F.; Zou, Y. P. *Adv. Mater.* **2008**, *20*, 2952–2958.
(7) Forrest, S. R. *MRS Bull.* **2005**, *30*, 28–32.
(8) Lu, G.; Li, L.; Yang, X. *Small* **2008**, *4*, 601–606.
(9) Lee, J. H.; Kim, D. W.; Jang, H.; Choi, J. K.; Geng, J.; Jung, J. W.; Yoon, S. C.; Jung, H. T. *Small* **2009**, *5*, 2139–43.
(10) He, X. M.; Gao, F.; Tu, G. L.; Hasko, D.; Huttner, S.; Steiner, U.; Greenham, N. C.; Friend, R. H.; Huck, W. T. S. *Nano Lett.* **2010**, *10*, 1302–1307.
(11) Coakley, K. M.; McGehee, M. D. *Chem. Mater.* **2004**, *16*, 4533–4542.
(12) Kumar, A.; Li, G.; Hong, Z. R.; Yang, Y. *Nanotechnology* **2009**, *20*, 165202.
(13) Oh, J. Y.; Jang, W. S.; Lee, T. I.; Myoung, J. M.; Baik, H. K. *Appl. Phys. Lett.* **2011**, *98*, 023303.
(14) Tan, Z. A.; Zhu, T.; Thein, M.; Gao, S. A.; Cheng, A.; Zhang, F.; Zhang, C. F.; Su, H. P.; Wang, J. K.; Henderson, R.; Hahm, J. I.; Yang, Y. P.; Xu, J. *Appl. Phys. Lett.* **2009**, *95*, 063510.
(15) Hsieh, C. H.; Cheng, Y. J.; Li, P. J.; Chen, C. H.; Dubosc, M.; Liang, R. M.; Hsu, C. S. *J. Am. Chem. Soc.* **2010**, *132*, 4887–4893.
(16) Drechsel, J.; Männig, B.; Kozlowski, F.; Gebeyehu, D.; Werner, A.; Koch, M.; Leo, K.; Pfeiffer, M. *Thin Solid Films* **2004**, *451–452*, 515–517.
(17) Ali, M.; Abbas, M.; Shah, S. K.; Tuerhong, R.; Generosi, A.; Paci, B.; Hirsch, L.; Gunnella, R. *Org. Electron.* **2012**, *13*, 2130–2137.
(18) Liang, C. W.; Su, W. F.; Wang, L. Y. *Appl. Phys. Lett.* **2009**, *95*, 133303.
(19) Kuo, T. H.; Chen, F. C.; Li, J. H.; Huang, A. T.; Huang, J. H.; Ho, K. C.; Chu, C. W. *J. Mater. Chem.* **2012**, *22*, 1364–1369.
(20) Sun, Y.; Chien, S. C.; Yip, H. L.; Zhang, Y.; Chen, K. S.; Zeigler, D. F.; Chen, F. C.; Lin, B. P.; Jen, A. K. Y. *Chem. Mater.* **2011**, *23*, 5006–5015.
(21) Kang, N. S.; Ju, B. K.; Lee, T. W.; Choi, D. H.; Hong, J. M.; Yu, J. W. *Sol. Energy Mater. Sol. Cells* **2011**, *95*, 2831–2836.
(22) Cheng, Y. J.; Hsieh, C. H.; He, Y. J.; Hsu, C. S.; Li, Y. F. *J. Am. Chem. Soc.* **2010**, *132*, 17381–17383.
(23) Chen, H.-Y.; Hou, J.; Zhang, S.; Liang, Y.; Yang, G.; Yang, Y.; Yu, L.; Wu, Y.; Li, G. *Nat. Photon.* **2009**, *3*, 649–653.
(24) Qian, D. P.; Xu, Q.; Hou, X. L.; Wang, F. Z.; Hou, J. H.; Tan, Z. A. *J. Polym. Sci., Part A: Polym. Chem.* **2013**, *51* (15), 3123–3131 (DOI: 10.1002/pola.26695).
(25) He, Y. J.; Zhao, G. J.; Peng, B.; Li, Y. F. *Adv. Funct. Mater.* **2010**, *20*, 3383–3389.
(26) Schmitz, I.; Schreiner, M.; Friedbacher, G.; Grasserbauer, M. *Appl. Surf. Sci.* **1997**, *115*, 190–198.
(27) Moulé, A. J.; Meerholz, K. *Adv. Mater.* **2008**, *20*, 240–245.

(28) Tan, Z. A.; Zhang, W. Q.; Cui, C. H.; Ding, Y. Q.; Qian, D. P.; Xu, Q.; Li, L. J.; Li, S. S.; Li, Y. F. *Phys. Chem. Chem. Phys.* **2012**, *14*, 14589−14595.
(29) Wang, F. Z.; Li, L. J.; Xu, Q.; Qian, D. P.; Li, S. S.; Tan, Z. A. *Org. Electron.* **2013**, *14*, 845−851.
(30) Markov, D. E.; Tanase, C.; Blom, P. W. M.; Wildeman, J. *Phys. Rev. B* **2005**, *72*, 045217.
(31) Theander, M.; Yartsev, A.; Zigmantas, D.; Sundström, V.; Mammo, W.; Andersson, M. R.; Inganäs, O. *Phys. Rev. B* **2000**, *61*, 12957−12963.
(32) Campoy-Quiles, M.; Ferenczi, T.; Agostinelli, T.; Etchegoin, P. G.; Kim, Y.; Anthopoulos, T. D.; Stavrinou, P. N.; Bradley, D. D. C.; Nelson, J. *Nat. Mater.* **2008**, *7*, 158−164.
(33) Clark, M. D.; Jespersen, M. L.; Patel, R. J.; Leever, B. J. *ACS Appl. Mater. Interfaces* **2013**, *5* (11), 4799−4807 (DOI: 10.1021/am4003777).
(34) Owens, D. K.; Wendt, R. *J. Appl. Polym. Sci.* **1969**, *13*, 1741−1747.